Magnetic CeO2/SrFe12O19 Nanocomposite: Synthesis, Characterization and Photocatalytic Degradation of Methyl Orange

Article · July 2022

DOI: 10.1007/s13369-022-07044-5

CITATIONS
0

READS
59

11 authors, including:

Saade Abdalkareem Jasim
Al-Maarif University College
122 PUBLICATIONS **201** CITATIONS
SEE PROFILE

Indrajit Patra
72 PUBLICATIONS **25** CITATIONS
SEE PROFILE

Moaed E. Algazally
University of Al-Ameed
135 PUBLICATIONS **135** CITATIONS
SEE PROFILE

Taif Alawsi
Al-Ayen University
93 PUBLICATIONS **40** CITATIONS
SEE PROFILE

Arabian Journal for Science and Engineering
https://doi.org/10.1007/s13369-022-07044-5

RESEARCH ARTICLE-CHEMISTRY

Magnetic $CeO_2/SrFe_{12}O_{19}$ Nanocomposite: Synthesis, Characterization and Photocatalytic Degradation of Methyl Orange

Saade Abdalkareem Jasim[1] · Indrajit Patra[2] · Ahmed M. Abdulhadi[3] · Moaed E. Al-Gazally[4] · Himanshu Sharma[5] · Taif Alawsi[6] · Halah T. Mohammed[7] · Shaymaa Abed Hussein[8] · Usama S. Altimari[9] · Ali Thaeer Hammid[10] · Cui Chem[11]

Received: 2 March 2022 / Accepted: 9 June 2022

Abstract
Magnetic nanocomposite $CeO_2/SrFe_{12}O_{19}$ including a hard magnetic material ($SrFe_{12}O_{19}$) and soft magnetic material (CeO_2) was prepared by a one-step chemical co-precipitation with high-temperature (900 °C) sintering method. Its structure and properties were studied using Fourier transform infrared (FT-IR), X-ray diffraction (XRD), vibrating-sample magnetometry (VSM), scanning electron microscope (SEM), energy-dispersive X-ray spectroscopy (EDS) and map analysis (MA). The testing results showed that the structure and phase of $SrFe_{12}O_{19}$ did not change by growth CeO_2 nanoparticles. SEM image and map analysis indicated that $SrFe_{12}O_{19}$ was distributed between the CeO_2 nanoparticles. Nanocomposite $CeO_2/SrFe_{12}O_{19}$ showed the quite high magnetic performance of 39.34 emu/g, indicating that the properties of $CeO_2/SrFe_{12}O_{19}$ were favorable to its separation, recycling and used after photocatalytic process without secondary pollution. In addition, the photocatalytic activity $CeO_2/SrFe_{12}O_{19}$ for the degradation of methyl orange (MO) was explored under UV light and results revealed the superior photocatalytic performance of MO dye with removal percentage of 88.38% within 90 min.

Keywords $CeO_2/SrFe_{12}O_{19}$ nanocomposite · Co-precipitation · Photocatalytic activity · Degradation

1 Introduction

Recently, the environmental pollution due to the rapid growth of different organic pollutions [1–3] of industrial activities has become a prominent issue with a detrimental influence on human life [4–6]. The organic pollutions are stable, non-biodegradable, toxic, carcinogenic and also lead to generation of dangerous by-products using different chemical reactions such as oxidation and hydrolysis [7, 8]. Among the various organic pollutions, the organic dyes such as Congo red [9], methyl orange [8, 10], methylene blue [11], rhodamine B [12] and rhodamine 6G [13] are promising and must be removed from wastewater before discharge to environment. Until now, different techniques such as physical, chemical and biological [14–16] were used to different dyes treatment. Among them, photocatalytic method has attracted more attention because of its low price, non-toxicity and high efficiency [17–19]. Nanostructured metal oxides such as CeO_2 [20], Fe_2O_3 [21] and TiO_2 [22] and their binary nanocomposites such as Bi_2O_3-Al_2O_3 [23], CeO_2-Bi_2WO_6 [24], CeO_2-TiO_2 [25] and TiO_2-ZnO [26] have attracted

✉ Cui Chem
cchem2021@gmail.com

1 Medical Laboratory Techniques Department, Al-Maarif University College, Al-anbar-Ramadi, Iraq

2 An Independent Researcher, NIT Durgapur, Durgapur, West Bengal, India

3 Civil Engineering Department, University of Warith Al-Anbiyaa, Karbala, Iraq

4 College of Medicine, University of Al-Ameed, Karbala, Iraq

5 Department of Computer Engineering and Applications, GLA University, Mathura, India

6 Scientific Research Center, Al-Ayen University, Thi-Qar, Iraq

7 Anesthesia Techniques Department, Al-Mustaqbal University College, Babylon, Iraq

8 Al-Manara College for Medical Sciences, Maysan, Iraq

9 Al-Nisour University College, Baghdad, Iraq

10 Computer Engineering Techniques Department, Faculty of Information Technology, Imam Ja'afar Al-Sadiq University, Baghdad, Iraq

11 Department of Chemistry, Xian University, Xian, China

Published online: 19 July 2022

much research interest and used in photocatalytic degradation of different organic dyes. Separation of catalyst from aqueous solution is difficult, then probably produced secondary pollution and also increased costs. To overcome these problems, usage of magnetic catalyst was proposed because of simple separation of them by an external magnet [23–26].

Hexaferrite strontium ferrite ($SrFe_{12}O_{19}$), as hard magnetic materials, has excellent properties such as large saturation magnetization, good chemical stability, superior coercivity and high uniaxial magnetic crystalline anisotropy [27–31]. In recent years, various binary $SrFe_{12}O_{19}$-based nanocomposites, such as $ZnFe_2O_4/SrFe_{12}O_{19}$ [32], β-$Bi_2O_3/SrFe_{12}O_{19}$ [33], $Bi_3O_4Cl/SrFe_{12}O_{19}$ [34], $SrFe_{12}O_{19}@Fe_3O_4$ [35], $CoFe_2O_4/SrFe_{12}O_{19}$ [36–38], MoS_2-$SrFe_{12}O_{19}$ [39] and BiOCl-$SrFe_{12}O_{19}$ [40], were synthesized and used in photocatalytic degradation of different organic dyes under light irradiation [32–34].

To the best of our knowledge, different magnetic composites based $SrFe_{12}O_{19}$ were synthesized using sol–gel [32, 38], hydrothermal [34, 35, 37], chemical co-precipitation [36] and characterized. But, there is less reported to binary and ternary composites-based $SrFe_{12}O_{19}$ with rare earth transition metal oxide like CeO_2 [18] and Bi_2O_3 [12, 33]. Therefore, in this paper, the $CeO_2/SrFe_{12}O_{19}$ binary composite magnetic photocatalyst was prepared by one-step chemical co-precipitation with high-temperature sintering method, characterized and the photocatalytic activity of was evaluated by methyl orange (MO) photodegradation.

2 Experimental

2.1 Materials and Characterization

All the chemical and reagents used in this paper were of high purity and were purchased from Merck and Sigma and used without further purification. FT-IR spectra were recorded on a 5DX FTIR spectrometer (Nicolet Co., USA), using KBr pellets in the range of 4000–400 cm^{-1}. The crystal structure and phases were identified via X-ray powder diffraction (XRD) using a Bruker Advance D8 diffractometer (Cu Kα radiation, $\lambda = 1.54056$ Å). The magnetic properties were investigated using a vibrating sample magnetometer (VSM, Meghnatis Daghigh Kavir Co., Iran) with applied magnetic field of up to 14 KOe. The morphologies of samples were recorded by scanning electron microscopy (SEM, JEOL-JSM 7600 F).

2.2 Synthesis of $CeO_2/SrFe_{12}O_{19}$ Nanocomposite

The $CeO_2/SrFe_{12}O_{19}$ nanocomposite was synthesized by one-step chemical co-precipitation with high-temperature sintering method. First mixed $Sr(NO_3)_2$ (0.211 g), $Ce(NO_3)_2{\bullet}9H_2O$ (0.868 g) and $Fe(NO_3)_3{\bullet}9H_2O$ (4.02 g) with molar ratio of 1:2:10 together. Then added the 50 mL distilled water and stirred for 20 min. After that, under vigorous stirring, the pH value of the solution is achieve to 12 by adding 0.5 M NaOH and the suspension was stirred at 70 °C for 24 h. Subsequently, the intermediate brown precipitates could be obtained using filtration, washing and drying. Then, the intermediate brown powder was ground by mortar in ceramic crucible and put into a muffle furnace, which was annealed at 900 °C for 3 h. The black powders washed, dried and characterized.

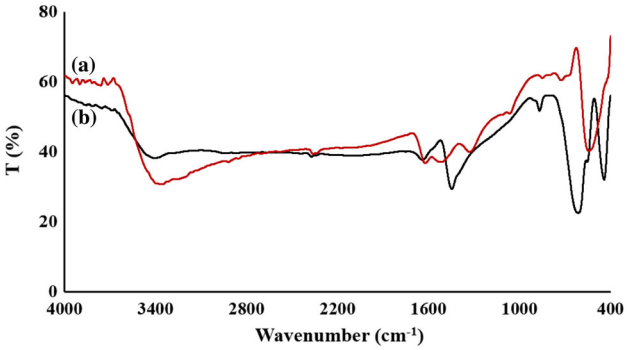

Fig. 1 FT-IR spectra of **a** CeO_2 and **b** $CeO_2/SrFe_{12}O_{19}$ nanocomposite

2.3 Photocatalytic Degradation of Methylene Blue

The photocatalytic activity of the $CeO_2/SrFe_{12}O_{19}$ was studied by the degradation of MO under UV light irradiation of a 300 W Xe lamp at the natural pH value. A 50 mL of 20 mg/L MO aqueous solution and suitable amount of $CeO_2/SrFe_{12}O_{19}$ (0.01 or 0.02 g) were added into container and stirred for 1 h in the dark. After that, the solution was irradiated by UV light. After a given time, about 4 mL of the mixture was withdrawn and the catalyst was separated using an external magnet. Then, the absorption of solution was monitored with a UV–Vis spectrophotometer. The photocatalytic experiments were conducted three times with statistically similar results each time. The degradation rate of MO was calculated by the following equation, where C_o and C_t represent the initial and different reaction time absorbance of MO.

$$R\,(\%) = \{(C_o - C_t) \times 100\} / C_o \quad (1)$$

3 Results and Discussions

3.1 FT-IR

The FT-IR spectrum of $CeO_2/SrFe_{12}O_{19}$ is shown in Fig. 1. It can be seen that the metal oxygen (Fe–O, Sr–O and Ce–O)

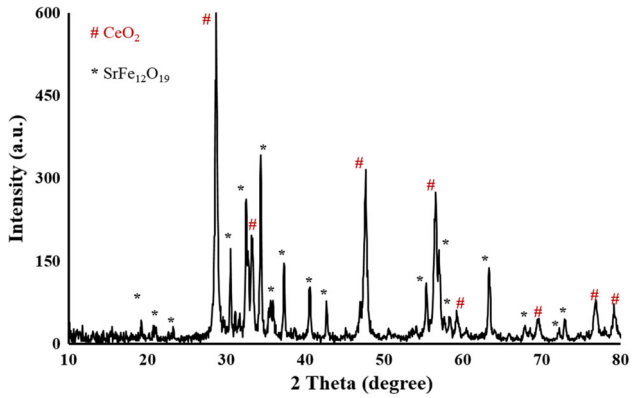

Fig. 2 XRD pattern of $CeO_2/SrFe_{12}O_{19}$ nanocomposite

stretching vibration frequencies of $SrFe_{12}O_{19}$ and CeO_2 appeared at 442 and 612 cm^{-1} [11, 21]. A peak appeared at 867 cm^{-1} confirms Ce–O stretching vibration [21, 41]. The peak observed at 1446 cm^{-1} suggests that the existence of stretching vibration of NO_3^- ion [21, 41] may be ascribed the remained of metal nitrate precursors. In addition, two broad peaks appeared at 1639 and 3420 cm^{-1} confirm the O–H bending and stretching vibration of water molecules adsorbed on the surface of $CeO_2/SrFe_{12}O_{19}$ nanocomposite [28, 32, 33].

3.2 XRD Pattern

Figure 2 illustrates the XRD pattern of $CeO_2/SrFe_{12}O_{19}$ nanocomposite. The characteristic peaks of $SrFe_{12}O_{19}$ were observed at 2θ values of 30.1, 32.1, 34.3, 36.5, 37.3, 41.2, 43.5, 55.7, 56.9, 63.2, 67.8 and 72.9° corresponds to (110), (107), (114), (201), (108), (205), (206), (217), (218), (220), (2014) and (317) crystallographic planes are precisely well matched to the pure hexagonal $SrFe_{12}O_{19}$ structure with JCPDS card no: 24–1207 [29, 32]. Also, the characteristic peaks of cubic CeO_2 nanoparticles were observed at 2θ values of 28.8, 33.1, 37.6, 56.7, 59.5, 69.9, 76.9 and 79.2° corresponding to charact corresponds to eristic (111), (200), (220), (311), (222), (400), (331), and (420) crystallographic plane well matched to the pure CeO_2 nanoparticles with JCPDS card no 34–0394 [21, 34, 42].

The average crystallite size of CeO_2 and $SrFe_{12}O_{19}$ nanoparticles was calculated using Debye–Scherrer formula based on the high intensity peaks appearing at 2θ value of 28.8° for CeO_2 and 34.3° for $SrFe_{12}O_{19}$ and was measured as 43.52 and 44.13 nm, respectively, which also agree well with the nanoparticle size shown in the SEM images (Fig. 3).

3.3 SEM Images

The morphology of $CeO_2/SrFe_{12}O_{19}$ nanocomposite is observed by using SEM images as represented in Fig. 3. The images confirms a spherical shape with a rough surface. The average particle size was distributed in the range of 25–50 nm. The molecular mass of $SrFe_{12}O_{19}$ was higher than that of CeO_2, confirms the $SrFe_{12}O_{19}$ particles absorbed more electron than CeO_2 particles and causes that the low molecular mass material (CeO_2) displayed more bright. Therefore, the $SrFe_{12}O_{19}$ regions were possibly dark [32].

3.4 EDX/elemental Mapping

Elemental analytical data (Sr, Ce, Fe and O) and distribution of them on $CeO_2/SrFe_{12}O_{19}$ nanocomposite were obtained by EDX/elemental mapping as represented in Figs. 4 and 5, respectively. Analysis was conducted at many different points and the atom percentage of each element is shown in the inset of Fig. 4. As seen in Fig. 5, the distribution of all atoms in $CeO_2/SrFe_{12}O_{19}$ nanocomposite is almost homogeny and confirms the preparation of core–shell $CeO_2/SrFe_{12}O_{19}$ nanocomposite.

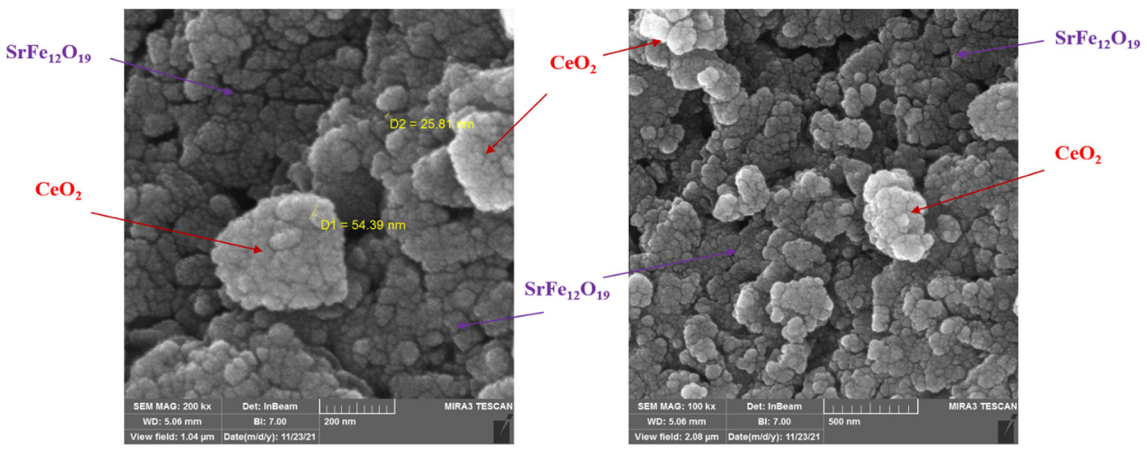

Fig. 3 SEM images of $CeO_2/SrFe_{12}O_{19}$ nanocomposite

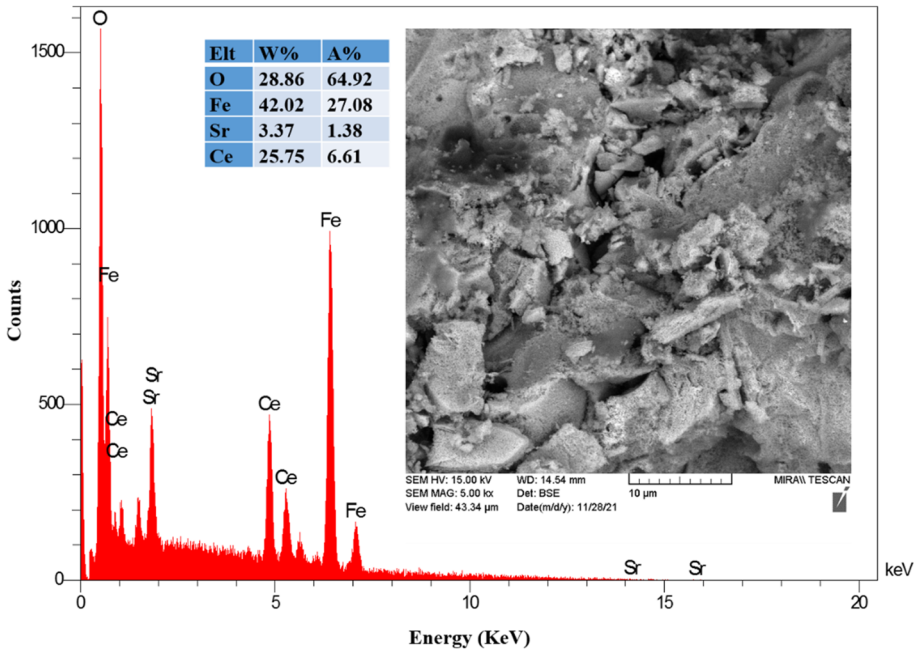

Fig. 4 EDS spectrum of $CeO_2/SrFe_{12}O_{19}$ nanocomposite

3.5 VSM

The magnetic hysteresis loop of $CeO_2/SrFe_{12}O_{19}$ nanocomposite is represented in Fig. 6. As shown in Fig. 6, the hysteresis loop area of $CeO_2/SrFe_{12}O_{19}$ nanocomposite is wide with saturation magnetization (M_s) of 39.34 emu/g, and a remnant magnetization (M_r) of 21.5 emu/g indicates that the sample is a kind of hard-magnetic materials [12, 32, 33]. The coercivity (H_c) of $CeO_2/SrFe_{12}O_{19}$ nanocomposite is 5384 Oe, indicating that it possesses a good anti-demagnetization ability, which was beneficial to its recycling from solution after used as photocatalyst using external magnet and also reused it again in photodegradation of different organic dyes such as methylene blue [32, 33] and rhodamine B [12, 34].

3.6 Photocatalytic Activity

Methyl orange is an aromatic anionic dye which is stable, toxic and colorant and causes serious environmentally problems [43, 44]. Then, removal of MO dye is a major environmental issue before discharging to receiving water using different route such as adsorption [45–47] and photocatalytic degradation [10, 20, 48]. Recently, photocatalytic degradation of MO has been applied by different compounds such as transition metal oxides Fe_2O_3 [20, 21, 30], ZnO [48] and TiO_2 [22], binary heterojunction Bi_2O_3-Al_2O_3 [23], AgBr/g-C_3N_4 [49] and TiO_2/ZnO [26], strontium hexaferrite [28], ternary heterojunction Ag/TiO_2/biochar [10], attapulgite-SnO_2-TiO_2 [50] AgBr@Ag_3PO_4/Fe_3O_4 [51] and PEDOT/NiO/Fly ash [52], CdS/CeO_2/Ag_3PO_4 [53] and also quaternary heterojunction PANI-CdS/CeO_2/Ag_3PO_4 [54].

The photocatalytic property of $CeO_2/SrFe_{12}O_{19}$ nanocomposite on photodegradation of MO under UV light was analyzed by monitoring of UV–Vis spectra of MO solution (Fig. 7). As seen in Fig. 7, the maximum value of absorbance peak of MO solution is observed at 472 nm that the peak only become decrease slowly with respect to the increases in irradiation time, confirming sufficient photocatalytic degradation of MO dye. Also, the peak did not shift and no other peaks were appeared, predicting that the pure photochemical reaction was happened [33].

3.7 Effect of Irradiation Time and Catalyst Dose

The influence of irradiation time and catalyst dose on photocatalytic performance of MO is represented in Fig. 8. In the first 5 min of irradiation time, about 32.12% and 43.46% of MO was degraded using 0.01 and 0.02 g of $CeO_2/SrFe_{12}O_{19}$ as photocatalyst, respectively. While at 90 min irradiation time, the percentage of MO photodegradation were 73.26 and 88.38%, respectively.

Compared with the photodegradation performance of other compounds (Table 1), it was noted that the $CeO_2/SrFe_{12}O_{19}$ exhibited remarkably better photocatalytic activity.

The photodegradation performance of $CeO_2/SrFe_{12}O_{19}$ was evaluated for 5 cycles. After each experiment, the photocatalyst collected by centrifuged, washed twice with distilled water, dried at 80 °C and then used for degradation of MO in similar conditions. Reusability performance results are

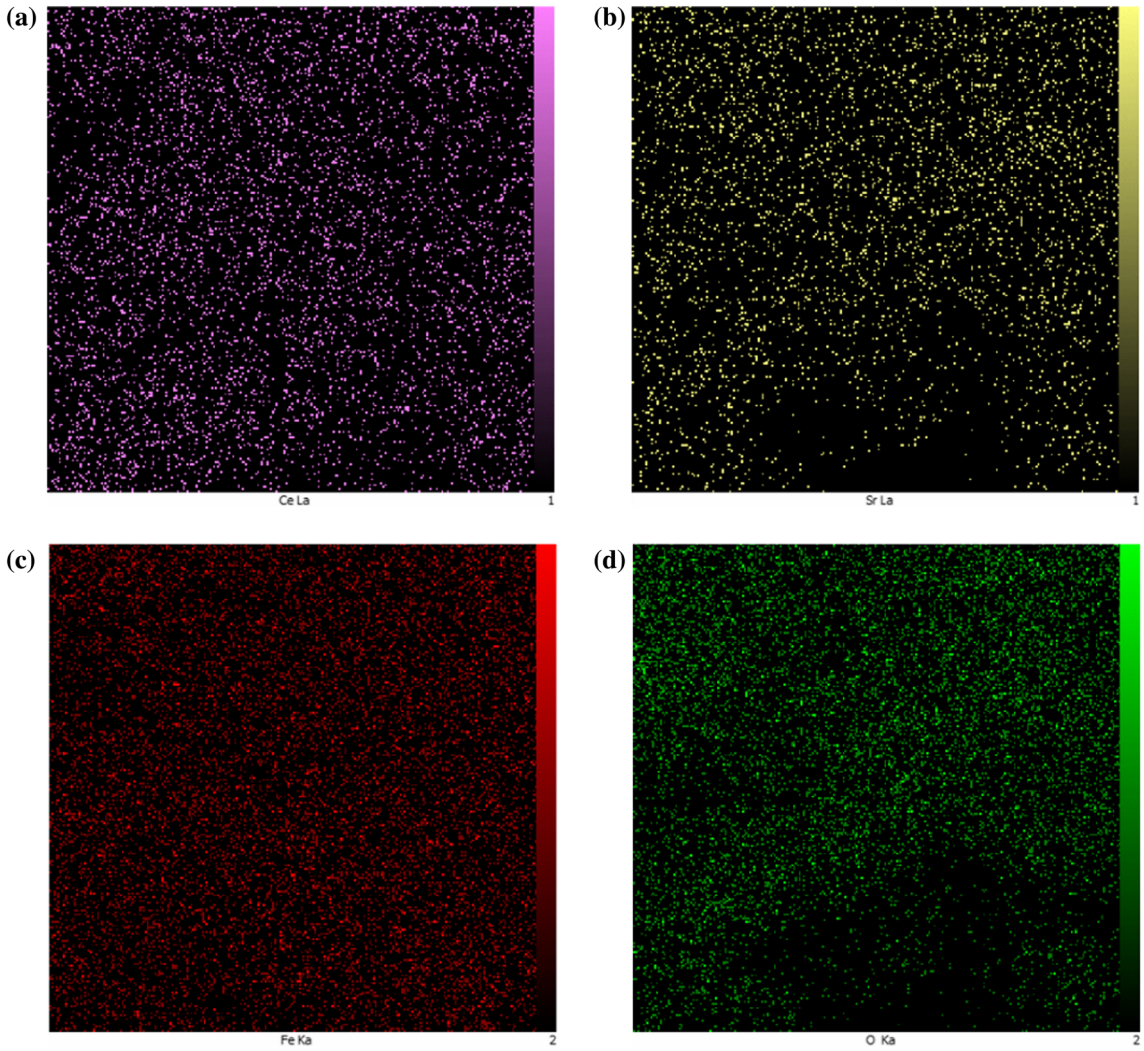

Fig. 5 Elemental distribution **a** Ce, **b** Sr, **c** Fe and **d** O images of $CeO_2/SrFe_{12}O_{19}$ nanocomposite

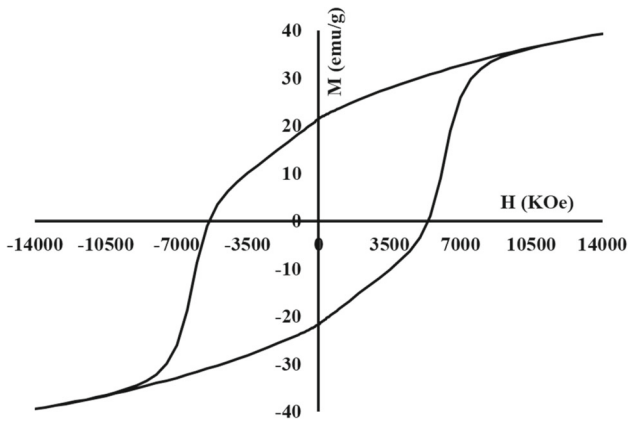

Fig. 6 Hysteresis loops of $CeO_2/SrFe_{12}O_{19}$ nanocomposite

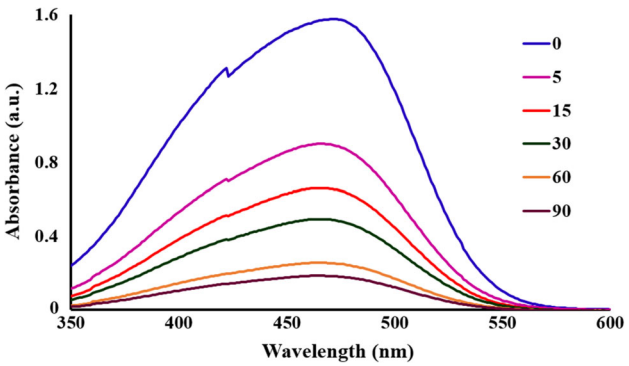

Fig. 7 Time-dependent UV–Vis spectra of MO solution in the presence of $CeO_2/SrFe_{12}O_{19}$ nanocomposite

shown in Fig. 9. As can be seen in Fig. 9, it was clear that $CeO_2/SrFe_{12}O_{19}$ as photocatalyst showed an excellent activity after 5 cycles and a slight amount (< 5%) in photodegradation activity was observed.

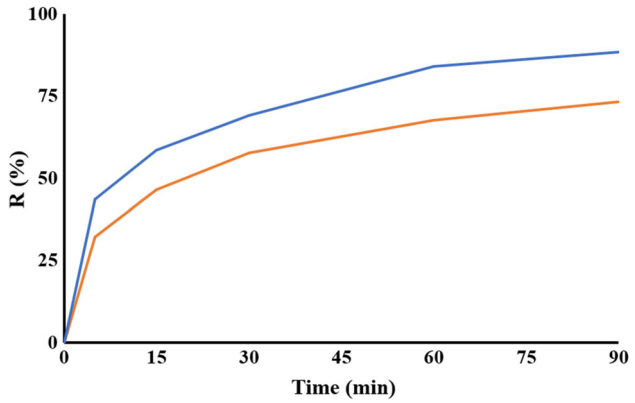

Fig. 8 The effect of irradiation time on removal percentage of MO dye in the presence of **a** 0.01 and **b** 0.02 g of $CeO_2/SrFe_{12}O_{19}$ nanocomposite

Table 1 The photodegradation performance of $CeO_2/SrFe_{12}O_{19}$ and other compounds

Adsorbent	Photodegradation percentage (%)	Reference
$CeO_2/SrFe_{12}O_{19}$	88.38	This work
Fe_2O_3	95%	[21]
TiO_2/ZnO	97%	[26]
Bi_2O_3-Al_2O_3	60	[23]
MoS_2/Fe_3O_4	79	[54]
TiO_2 powder	24	[22]
Ag/TiO_2/biochar	97.5	[10]
α-Fe_2O_3@carbon core–shell	85	[55]
$SrFe_{12}O_{19}$	95	[28]

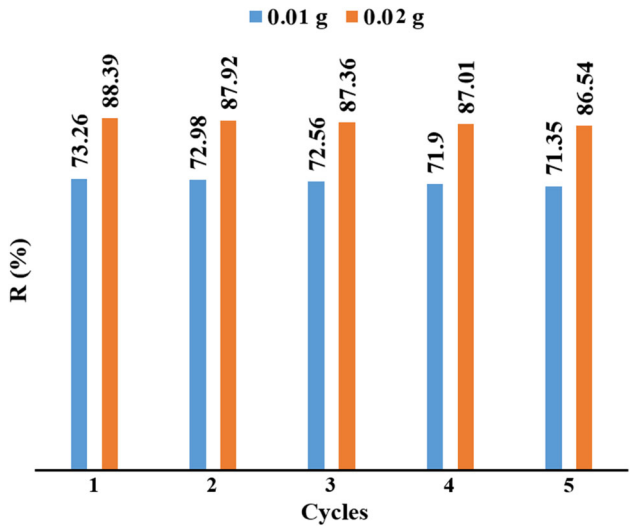

Fig. 9 Reusability experiment of $CeO_2/SrFe_{12}O_{19}$ nanocomposite for 5 cycles

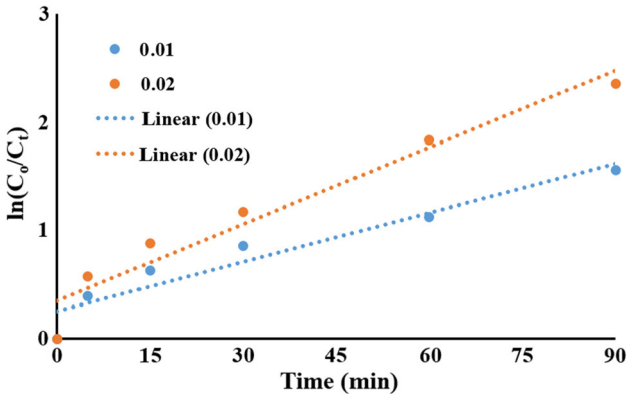

Fig. 10 Pseudo-first-order plots of MO degradation of **a** 0.01 and **b** 0.02 g of $CeO_2/SrFe_{12}O_{19}$ nanocomposite

3.8 Longmuir Isotherm

The kinetic analysis of the degradation of MO dye using $CeO_2/SrFe_{12}O_{19}$ nanocomposite by Langmuir model was investigated and the linear relationship between $\ln(C_o/C_t)$ and time is confirmed by pseudo first-order kinetic as shown in Fig. 10.

A suitable mechanism for the photodegradation of methyl orange using $CeO_2/SrFe_{12}O_{19}$ nanocomposite was proposed based on the above results, as demonstrated by following equations [11, 21, 28, 30, 32]:

$$CeO_2/SrFe_{12}O_{19} + h\nu \rightarrow e^-(CeO_2) + h^+(SrFe_{12}O_{19}) \quad (2)$$

$$e^-(CeO_2) + O_2 \rightarrow O_2^{\circ -} \quad (3)$$

$$h^+(SrFe_{12}O_{19}) + H_2O \rightarrow H^\circ + OH^\circ \quad (4)$$

$$H^\circ + O_2^{\circ -} + OH^\circ + MO \rightarrow \text{degradation products} \quad (5)$$

For photodegradation of organic dyes using different photocatalysts, there are several steps [28] such as diffusion and adsorption of dye on the surface of catalyst, adsorption of light by catalyst for preparation of e^-/h^+ pair (charge separation), various reactions to produce active radicals and finally degradation of dye by active radicals H°, $O_2^{\circ -}$ and OH° [11, 21, 28, 30, 32].

4 Conclusions

We have successfully prepared a magnetic nanocomposite $CeO_2/SrFe_{12}O_{19}$ photocatalyst by a one-step chemical co-precipitation with high-temperature sintering method. High magnetic performance of $CeO_2/SrFe_{12}O_{19}$ predicts the ease separation of $CeO_2/SrFe_{12}O_{19}$, to its recycling and reused

without secondary pollution. The photocatalytic potential of $CeO_2/SrFe_{12}O_{19}$ illustrated that the percentage of MO degradation was up to 88.38% after UV light irradiation for 90 min. The photocatalytic data revealed that the degradation of MO followed by Langmuir isotherm as pseudo-first-order kinetic model.

Author Contribution S.A. Jasim, A.M. Abdulhadi, M.E. Al-Gazally and T. Alawsi collected the FT-IR, XRD and VSM analysis, revised the paper. I. Patra and H. Sharma revised the paper, recorded the SEM/EDX and DSC analysis. H.T. Mohammed, S.A. Hussein, U.S. Altimari, A.T. Hammid designed and collected the photodegradation data, revised the paper. C. Chem supervised, wrote and revised the paper. All authors discussed the results and contributed to the final manuscript.

Declarations

Conflict of interest The authors declare that there is no conflict of interest.

References

1. He, L.; Yang, C.; Ding, J.; Lu, M.; Chen, C.; Wang, G.; Yang, S.S.: Fe, N-doped carbonaceous catalyst activating periodate for micropollutant removal: Significant role of electron transfer. Appl. Catal. B Environ. **303**, 120880 (2022)
2. Li, G.; Huang, S.; Zhu, N.; Yuan, H.; Ge, D.; Wei, Y.: Defect-rich heterojunction photocatalyst originated from the removal of chloride ions and its degradation mechanism of norfloxacin. Chem. Eng. J. **421**, 127852 (2021)
3. Li, G.; Huang, S.; Zhu, N.; Yuan, H.; Ge, D.: Near-infrared responsive upconversion glass-ceramic@BiOBr heterojunction for enhanced photodegradation performances of norfloxacin. J. Hazard. Mater. **403**, 123981 (2021)
4. Liu, Y.; Zhang, Q.; Yuan, H.; Luo, K.; Li, J.; Hu, W.; Bazaka, K.: Comparative study of photocatalysis and gas sensing of ZnO/Ag nanocomposites synthesized by one- and two-step polymer-network gel processes. J. All. Compd. **868**, 158723 (2021)
5. Cheng, J.; Tan, Z.; Xing, Y.; Shen, Z.; Zhang, Y.; Liu, L.; Liu, S.: Exfoliated conjugated porous polymer nanosheets for highly efficient photocatalytic hydrogen evolution. J. Mater. Chem. A Mater. Energy Sustain. **9**, 5787–5795 (2021)
6. Chen, F.; Ma, J.; Zhu, Y.; Li, X.; Yu, H.; Sun, Y.: Biodegradation performance and anti-fouling mechanism of an ICME/electro-biocarriers-MBR system in livestock wastewater (antibiotic-containing) treatment. J. Hazard. Mater. **426**, 128064 (2022)
7. Chen, C.; Yang, S.; Ding, J.; Wang, G.; Zhong, L.; Zhao, S.; Ren, N.: Non-covalent self-assembly synthesis of AQ2S@rGO nanocomposite for the degradation of sulfadiazine under solar irradiation: The indispensable effect of chloride. Appl. Catal B Environ. **298**, 120495 (2021)
8. Naikwade, A.G.; Jagadale, M.B.; Kale, D.P.; Gophane, A.D.; Garadkar, K.M.; Rashinkar, G.S.: Photocatalytic degradation of methyl orange by magnetically retrievable supported ionic liquid phase photocatalyst. ACS Omega **5**, 131–144 (2020)
9. You, J.; Liu, C.; Feng, X.; Lu, B.; Xia, L.; Zhuang, X.: In situ synthesis of ZnS nanoparticles onto cellulose/chitosan sponge for adsorption–photocatalytic removal of Congo red. Carbohydr. Polym. **288**, 119332 (2022)
10. Shan, R.; Lu, L.; Gu, J.; Zhang, Y.; Yuan, H.; Chen, Y.; Luo, B.: Photocatalytic degradation of methyl orange by Ag/TiO_2/Biochar composite catalysts in aqueous solution. Mater. Sci. Semiconduct. Process. **114**, 105088 (2020)
11. Vatanparast, M.; Saeidi, L.: Sonochemical-assisted synthesis and characterization of CeO_2 nanoparticles and its photocatalytic properties. J Mater. Sci: Mater. Electron. **29**, 7107–7113 (2018)
12. Xie, T.; Yang, J.; Peng, Y.; Wang, J.; Liu, S.; Xu, L.; Liu, C.: β-$Bi_2O_3/SrFe_{12}O_{19}$ magnetic photocatalyst: facile synthesis and its photcatalytic activity. Mater. Technol. **34**, 843–850 (2019)
13. Madkour, M.; Allam, O.G.; Abdel Nazeer, A.; Amin, M.O.; Al-Hetlani, E.: CeO_2-based nanoheterostructures with p-n and n-n heterojunction arrangements for enhancing the solar-driven photodegradation of rhodamine 6G dye. J. Mater. Sci: Mater. Electron. **30**, 10857–10866 (2019)
14. Katheresan, V.; Kansedo, J.; Lau, S.Y.: Efficiency of various recent wastewater dye removal methods: A review. J. Environ. Chem. Eng. **6**, 4676–4697 (2018)
15. Sharma, S.; Kaur, A.: Various methods for removal of dyes from industrial effluents-A review. Ind. J. Sci. Technol. **11**, 1–21 (2018)
16. Bożęcka, A.M.; Orlof-Naturalna, M.M.; Kopeć, M.: Methods of dyes removal from aqueous environment. J. Ecol. Eng. **22**, 111–118 (2021)
17. Yan, H., Zhao, M., Feng, X., Zhao, S., Zhou, X., Li, S., Yang, C.: PO_4^{3-} coordinated robust single-atom platinum catalyst for selective polyol oxidation. ANGEWANDTE CHEMIE-INT. e.202116059 (2022)
18. Wang, S.; Gao, H.; Fang, L.; Hu, Q.; Sun, G.; Chen, X.; Yang, H.: Synthesis of novel CQDs/CeO2/SrFe12O19 magnetic separation photocatalysts and synergic adsorption-photocatalytic degradation effect for methylene blue dye removal. Chem. Eng. J. Adv. **6**, 100089 (2021)
19. Ziaadini, F.; Mostafavi, A.; Shamspur, T.; Fathirad, F.: Photocatalytic degradation of methylene blue from aqueous solution using $Fe_3O_4@SiO_2@CeO_2$ core-shell magnetic nanostructure as an effective catalyst. Adv. Environ. Technol. **2**, 127–132 (2019)
20. Gnanam, S.; Rajendran, V.: Facile sol-gel preparation of Cd-doped cerium oxide (CeO_2) nanoparticles and their photocatalytic activities. J. All. Compd. **735**, 1854–1862 (2018)
21. Khalaji, A.D.; Machek, P.; Jarosova, M.: α-Fe_2O_3 nanoparticles: Synthesis, characterization, magnetic properties and photocatalytic degradation of methyl orange. Adv. J. Chem. A **4**, 317–326 (2021)
22. Bian, Y.; Zheng, G.; Ding, W.; Hu, L.; Sheng, Z.: Magnetic field effect on the photocatalytic degradation of methyl orange by commercial TiO_2 power. RSC Adv. **11**, 6284–6291 (2021)
23. Hakimi, M.; Morvaridi, M.; Hosseini, H.A.; Alimard, P.: Preparation, characterization, and photocatalytic activity of Bi_2O_3-Al_2O_3 nanocomposite. Polyhedron **170**, 523–529 (2019)
24. Issarapanacheewin, S.; Wetchakun, K.; Phanichphant, S.; Kangwansupamonkon, W.; Wetchakun, N.: Efficient photocatalytic degradation of rhodamine B by a novel CeO_2/Bi_2WO_6 composite film. Catal. Today **278**, 280–290 (2016)
25. Kumar, S.S.; Lellala, K.; Ashok, M.; Piryadharsan, A.; Sanjeeviraja, C.; Rajendran, A.: Green synthesis of CeO_2-TiO_2 compound using Cleome chelidonii leaf extract for excellent photocatalytic activity. J. Mater. Sci: Mater. Elect. **29**, 14022–14030 (2018)
26. Zha, R.; Nadimicherla, R.; Guo, X.: Ultraviolet photocatalytic degradation of methyl orange by nanostructured TiO_2/ZnO heterojunctions. J. Mater. Chem. A **3**, 6565–6574 (2015)
27. Jing, P.; Du, J.; Wang, J.; Wei, J.; Pan, L.; Li, J.; Liu, Q.: Width-controlled M-type hexagonal strontium ferrite ($SrFe_{12}O_{19}$) nanoribbons with high saturation magnetization and superior coercivity synthesized by electrospinning. Sci. Rep. **5**, 15089 (2015)
28. Mohammadi, K.; Sadeghi, M.; Azimirad, R.: Facile synthesis of $SrFe_{12}O_{19}$ nanoparticles and its photocatalyst application. J. Mater. Sci: Mater. Electron. **27**, 10042–10047 (2017)

29. Sahoo, J.K.; Konar, M.; Rath, J.; Kuimar, D.; Sahoo, H.: Hexagonal strontium ferrite: cationic dye adsorption and antibacterial activity. Sep. Sci. Technol. **55**, 415–430 (2020)
30. Bayla, A.: Solvothermal synthesis of pure $SrFe_{12}O_{19}$ hexaferrite nanoplatelets. J. Supercond. Nov, Magn. **27**, 877–880 (2014)
31. Hedayati, K.; Behesht-Ara, Z.; Ghanbari, D.: Preparation and characterization of various morphologies of $SrFe_{12}O_{19}$ nano-structures: investigation of magnetization and coercivity. J. Mater. Sci: Mater. Electron. **28**, 1–9 (2017)
32. Xie, T.; Xu, L.; Liu, C.; Wang, Y.: Magnetic composite $ZnFe_2O_4$/$SrFe_{12}O_{19}$: preparation, characterization, and photocatalytic activity under visible light. Appl. Surface Sci. **273**, 684–691 (2013)
33. Xie, T.; Liu, C.; Xu, L.; Yang, J.; Zhou, W.: Novel heterojunction Bi_2O_3/$SrFe_{12}O_{19}$ magnetic photocatalyst with highly enhanced photocatalytic activity. J. Phys. Chem. C **117**, 24601–24610 (2013)
34. Wang, H.; Xu, L.; Liu, C.; Jiang, Z.; Feng, Q.; Wu, T.; Wang, R.: A novel magnetic photocatalyst Bi3O4Cl/SrFe12O19: fabrication, characterization and its photocatalytic activity. Cer. Internat. **46**, 460–467 (2020)
35. Viet Nga, T.T.; Thi Lan, N.: Fabrication and exchange-spring properties of $SrFe_{12}O_{19}$@Fe_3O_4 nanocomposites with core-shell structure. Mater. Chem. Phys. **251**, 123084 (2020)
36. Dhabekar, K.; Mohan Kant, K.: Preparation and magnetization dynamics of $CoFe_2O_4$-$SrFe_{12}O_{19}$ nanocomposites. J. Mater. Sci: Mater. Electron. **30**, 21011–21017 (2019)
37. Rezaei, E.; Rezanezhad, A.; Hajalilou, A.; Saleh Ghadimi, L.; Abouzari-Lotf, E.; Arsalani, N.: Electrochemical behavior of $SrFe_{12}O_{19}$/$CoFe_2O_4$ composite nanoparticles synthesized via one-pot hydrothermal method. J. All. Compd. **789**, 40–47 (2019)
38. Maltoni, P.; Sarkar, T.; Barucca, G.; Varvaro, G.; Locardi, F.; Peddis, D.; Mathieu, R.: Tuning the magnetic properties of hard-soft $SrFe_{12}O_{19}$@$CoFe_2O_4$ nanostructures via composition/interphase coupling. J. Phys. Chem. C **125**, 5927–5936 (2021)
39. Lu, Y.; Xu, L.; Liu, C.: Magnetically separable and recyclable photocatalyst MoS2-SrFe12O19 with p-n heterojunction: Fabrication, characterization, and photocatalytic mechanism. Appl. Organomet. Chem. **34**(1), 5288 (2020)
40. Xie, T.; Xu, L.; Liu, C.; Yang, J.; Wang, M.: Magnetic composite BiOCl–$SrFe_{12}O_{19}$: a novel p–n type heterojunction with enhanced photocatalytic activity. Dalton Trans. **43**, 2211–2220 (2014)
41. Negi, K.; Kumar, M.; Singh, G.; Chauhan, S.; Chauhan, M.S.: Nanostructured CeO_2 for selective-sensing and smart photocatalytic applications. Cer. Int. **44**, 15281–15289 (2018)
42. Saadoon, S.J.; Jarosova, M.; Machek, P.; Kadhim, M.M.; Ali, M.H.; Khalaji, A.D.: Methylene blue photodegradation using as-synthesized CeO2 nanoparticles. J. Chinese Chem. Soc. **69**(2), 280–288 (2022)
43. Yuvaraja, G.; Chen, D.Y.; Pathak, J.L.; Long, J.; Subbaiah, M.V.; Wen, J.C.; Pan, C.L.: Preparation of novel aminated chitosan schiff's base derivative for the removal of methyl orange dye from aqueous environment and its biological applications. Int. J. Biol. Macromol. **146**, 1100–1110 (2020)
44. Janani, B.; Al-Mohaimeed, A.M.; Raju, L.L.; Al Farraj, D.A.; Thomas, A.M.; Khan, S.S.: Synthesis and characterizations of hybrid PEG-Fe_3O_4 nanoparticles for the efficient adsorptive removal of dye and antibacterial, and antibiofilm applications. J. Environ. Health Sci. Eng. **19**, 389–400 (2021)
45. Lafi, R.; Hafiane, A.: Removal of methyl orange (MO) from aqueous solution using cationic surfactants modified coffee waste (MCWs). J. Taiwan Inst. Chem. Eng. **58**, 424–433 (2016)
46. Iwuozor, K.O.; Ighalo, J.O.; Emenike, E.C.; Ogunfowora, L.A.; Igwegbe, C.A.: Adsorption of methyl orange: A review on adsorbent performance. Curr. Res. Green Sustain Chem. **4**, 100179 (2021)
47. Debnath, A.; Chattopadhyay, K.K.; Saha, B.: Methyl orange adsorption onto simple chemical route synthesized crystalline α-Fe2O3 nanoparticles: kinetic, equilibrium isotherm, and neural network modeling. Desalin. Water Treat **57**, 13549–13560 (2016)
48. Isai, K.A.; Shrivastava, V.S.: Photocatalytic degradation of methyl orange using ZnO and Fe doped ZnO: A comparative study. Iran J. Catal. **9**, 259–268 (2019)
49. Ghattavi, S.; Nezamzadeh-Ejhieh, A.: A visible light driven AgBr/g-C_3N_4 photocatalyst composite in methyl orange photodegradation: Focus on photoluminescence, mole ratio, synthesis method of g-C_3N_4 and scavengers. Compos. B Eng. **183**, 107712 (2020)
50. Zhang, L.; Lv, F.; Zhang, W.; Li, R.; Zhong, H.; Zhao, Y.; Zhang, Y.; Wang, X.: Photodegradation of methyl orange by attapulgite-SnO_2-TiO_2 nanocomposites. J. Hazard. Mater. **171**, 294–300 (2009)
51. Wang, Z., Yin, L., Chen, Z., Zhou, G., Shi, H.: Photodegradation of methyl orange using magnetically recoverable AgBr@Ag_3PO_4/Fe_3O_4 photocatalyst under visible light. Nanomate. Environ. Appl. 150150 (2014)
52. Dagar, A.; Narula, A.K.: Photo-degradation of methyl orange under visible light by PEDOT/NiO/Fly ash cenosphere. Mater. Chem. Phys. **183**, 561–570 (2016)
53. Taddesse, A.M.; Bekele, T.; Diaz, I.; Adgo, A.: Polyaniline supported CdS/CeO_2/Ag_3PO_4 nanocomposite: An "A-B" type tandem n-n heterojunctions with enhanced photocatalytic activity. J. Photochem. Photobiol. A Chem. **406**, 113005 (2021)
54. Lin, C.; Wang, X.; Zhou, Q.; Wen, C.; Su, S.; Xiang, J.; Cheng, P.; Hu, X.; Li, Y.; Wang, X.; Gao, X.; Nozel, R.; Zhou, G.; Zhang, Z.; Liu, J.: Magnetically recyclable MoS_2/Fe_3O_4 hybrid composite as visible light responsive photocatalyst with enhanced photocatalytic performance. ACS Sustain. Chem. Eng. **7**, 1673–1682 (2019)
55. Munusamy, G.; Mani, R.; Varadharajan, K.; Narasimhan, S.; Munusamy, C.; Chandrasekaran, B.: α-Fe_2O_3@carbon core-shell nanostructure for luminescent upconversion and photocatalytic degradation of methyl orange. Res. Chem. Intermed. **46**, 715–736 (2020)